PNAS RESEARCH ARTICLE | CHEMISTRY

Photosynthetic biohybrid coculture for tandem and tunable CO_2 and N_2 fixation

Stefano Cestellos-Blanco[a,b], Rachel R. Chan[c], Yue-xiao Shen[b,c,1], Ji Min Kim[a,b], Tom A. Tacken[c,d], Rhesa Ledbetter[b,e,2], Sunmoon Yu[a,f], Lance C. Seefeldt[b,e], and Peidong Yang[a,b,c,f,g,3]

Contributed by Peidong Yang; received December 14, 2021; accepted April 25, 2022; reviewed by Neel Joshi and Chong Liu

Solar-driven bioelectrosynthesis represents a promising approach for converting abundant resources into value-added chemicals with renewable energy. Microorganisms powered by electrochemical reducing equivalents assimilate CO_2, H_2O, and N_2 building blocks. However, products from autotrophic whole-cell biocatalysts are limited. Furthermore, biocatalysts tasked with N_2 reduction are constrained by simultaneous energy-intensive autotrophy. To overcome these challenges, we designed a biohybrid coculture for tandem and tunable CO_2 and N_2 fixation to value-added products, allowing the different species to distribute bioconversion steps and reduce the individual metabolic burden. This consortium involves acetogen *Sporomusa ovata*, which reduces CO_2 to acetate, and diazotrophic *Rhodopseudomonas palustris*, which uses the acetate both to fuel N_2 fixation and for the generation of a biopolyester. We demonstrate that the coculture platform provides a robust ecosystem for continuous CO_2 and N_2 fixation, and its outputs are directed by substrate gas composition. Moreover, we show the ability to support the coculture on a high–surface area silicon nanowire cathodic platform. The biohybrid coculture achieved peak faradaic efficiencies of 100, 19.1, and 6.3% for acetate, nitrogen in biomass, and ammonia, respectively, while maintaining product tunability. Finally, we established full solar to chemical conversion driven by a photovoltaic device, resulting in solar to chemical efficiencies of 1.78, 0.51, and 0.08% for acetate, nitrogenous biomass, and ammonia, correspondingly. Ultimately, our work demonstrates the ability to employ and electrochemically manipulate bacterial communities on demand to expand the suite of CO_2 and N_2 bioelectrosynthesis products.

CO_2 electrosynthesis | bacterial coculture | N_2 electrosynthesis | biocatalysis

Significance

Combining (photo)electrochemical platforms with CO_2 -fixing bacteria as "living" biocatalysts has realized the highly selective reduction of CO_2 to C_{2+} products, such as acetate. This approach also enables the downstream conversion of the initial CO_2 product to a higher-value one. We report an advance on this concept by coculturing primary CO_2-fixing bacteria producing acetate with secondary N_2-fixing bacteria that employ the acetate to reduce N_2 to NH_3 and to generate a bioplastic. The symbiotic coculture can be controlled electrochemically and modularly tuned to generate a desired product stream. We foresee that this platform could be expanded to produce several additional products, including bioplastics, biofuels, and sugars, from only CO_2, N_2, H_2O, and electricity.

Society at large has benefitted from industrial chemical processes that rely heavily on hydrocarbon fossil fuels as both a source of energy and a feedstock. For example, steam methane reforming from natural gas is a key step to produce syngas consequently reacted with N_2 during the Haber–Bosch process to produce NH_3 commonly used as a fertilizer (1). However, as complications of exploiting nonrenewable hydrocarbon fuels exemplified by climate change and environmental pollution become more salient, we are pressed to find renewable alternatives that also close the carbon cycle by utilizing CO_2 (2). Efforts to reduce CO_2 through biological and electrochemical means are flourishing in both academia and industry (3–5). Microbial electrosynthesis, in particular, marries the advantages of electrochemistry and biology by electrifying microbial "living" catalysts to form chemicals from CO_2, N_2, and H_2O building blocks (6, 7). Microbes offer high product selectivity, low substrate activation barriers, self-construction, and regeneration (8). Meanwhile, electrochemistry often involves modular and light-activated nanocatalysts and can be easily powered by renewable solar energy (9, 10). Photosynthetic biohybrid systems (PBSs) driven by solar energy represent a promising strategy for sustainable chemical production (11).

Autotrophic bacteria, commonly *Sporomusa ovata*, accept reducing equivalents in the form of hydrogen or electrons from a poised cathode in an electrochemical cell (12). *S. ovata* in particular routinely converts CO_2 to acetate with over 80% faradaic efficiency (FE) using photo- and electrochemical reducing equivalents (13). Advances of this concept have broadly been achieved through genetic engineering (14, 15), adaptation of biocatalysts (16), and refinement of the electrochemical environment to increase biocompatibility (17). Our group previously established a solar-driven Si nanowire platform that allows for high loading capacity of *S. ovata* (18). When close packed with *S. ovata*, this platform enables a current density of 0.65 mA/cm^2 and a solar to chemical conversion efficiency of 3.6% (17). Despite steady improvements, the rate of CO_2 to acetate bioelectrosynthesis still lags behind those achieved by purely inorganic metal–based electrocatalysts by an order of magnitude due in part to the sluggish autotrophic metabolism of CO_2-fixing bacteria (19, 20). Therefore, we must emphasize

Author contributions: S.C.-B., L.C.S., and P.Y. designed research; S.C.-B., R.R.C., Y.S., J.M.K., T.A.T., R.L., and S.Y. performed research; S.C.-B. and P.Y. analyzed data; and S.C.-B., L.C.S., and P.Y. wrote the paper.

Reviewers: N.J., Northeastern University; and C.L., University of California, Los Angeles.

Competing interest statement: One of the referees of this manuscript, C.L., has coauthored with S.C.-B. and P.Y. in *J. Am. Chem. Soc.* **140**, 1978–1985 (2018) and *Chem. Rev.* **119**, 9221–9259 (2019).

[1]Present address: Department of Civil, Environmental, and Construction Engineering, Texas Tech University, Lubbock, TX 79430.

[2]Present address: Department of Biology, Hastings College, Hastings, NE 68901.

[3]To whom correspondence may be addressed. Email: p_yang@berkeley.edu.

This article contains supporting information online at http://www.pnas.org/lookup/suppl/doi:10.1073/pnas.2122364119/-/DCSupplemental.

Published June 21, 2022.

and build upon inherent advantages of the biocatalyst-based system (i.e., its high product selectivity and low substrate activation barrier) in order to continue moving the field forward in an impactful manner.

Long-term stability is customarily achieved by bioelectrosynthetic systems, which is particularly critical when their products are required as feedstocks for downstream processes. Their durability also facilitates productive long-term solar to chemical conversion (17). Furthermore, another pivotal advantage lies in the ability of microorganisms to produce higher-value carbon products through tandem biocatalysis. Liu et al. (18) used acetate from a PBS as a feedstock for genetically engineered *Escherichia coli* to produce biofuels, a bioplastic, and a pharmaceutical that are not attainable via inorganic CO_2 electrocatalysis. Their research establishes acetate as an upgradeable carbon intermediate that can be easily passed on to a second more specialized biocatalyst. The concept of using a bacterial community for tandem biocatalysis has been advanced to expand the suite of CO_2 carbon products (21–24), to enhance CO_2 fixation rates (25, 26), and even to increase the rate of current production in electrogenesis (27). Altogether, the coculturing of bacterial catalysts has centered on CO_2 fixation and carbon-based upgrading. As a progression, we hypothesize 1) that acetate cannot only be used as an upgradeable carbon intermediate but also, as an energy-rich substrate to power N_2 biocatalysis and 2) that we can exercise electrochemical control on a bacterial coculture.

Industrial N_2 fixation occurs primarily through the Haber–Bosch process to produce NH_3, commonly used as fertilizer to match the agricultural needs of an expanding global population. Ammonia has also been proposed as a carbon free energy carrier that is less volatile than H_2 (28). However, the Haber–Bosch process accounts for 1% of the world's energy use, releases harmful greenhouse gases, and pollutes the local environment (1). Additionally, transporting ammonia products from a centralized plant adds cost and generates carbon emissions, particularly to unindustrialized locales (29). N_2 electrocatalysis attempts to overcome the aforementioned issues by electrochemically reducing N_2 to NH_3 mediated by inorganic nanostructured catalysts to be powered with renewably solar energy at a decentralized scale (30). While significant strides have recently been reported (31, 32), these efforts are hampered by the nonspecificity of catalysts as evidenced by competing H_2 evolution (33), low overall yields (34), short durability (35), and complicated nanocatalyst synthesis often with precious metals (33–37).

To overcome some of these challenges, diazotrophic whole-cell bacteria have been harnessed for bioelectrochemical N_2 fixation (38, 39). More recent advances detail the tuning of the O_2 microenvironment to enhance bioelectrochemical N_2 fixation by a perfluorocarbon nanoemulsion or through a silicon-based microwire array (40, 41). Additionally, Dong et al. (42) reported an engineered cyanobacterium that directly uptakes electrons from a cathode for N_2 to NH_3 conversion. Nevertheless, certain obstacles may still hinder the efficiency and productivity of bioelectrochemical N_2 fixation; N_2 fixation is paired with sluggish autotrophic metabolism in a single bacterial species, which limits the rate of nitrogen fixation, and any generated ammonia is immediately consumed by the bacteria, resulting in nitrogenous cell biomass whose refinement is nontrivial if the desired product is ammonia. Furthermore, bioelectrochemical N_2 fixation systems employing single bacterial species commonly use evolved H_2 as a charge mediator, but H_2 has been reported to attenuate nitrogenase activity (43, 44).

We surmounted these challenges by coculturing individual specialized CO_2- and N_2-fixing microorganisms. We identified *Rhodopseudomonas palustris*, a purple nonsulfur bacterium capable of engaging versatile metabolic modes (45). *R. palustris* rapidly proliferated diazotrophically using acetate provided by *S. ovata* while also producing poly(3-hydroxybutyrate) (PHB), a biopolymer directly employed in additive manufacturing (46). Furthermore, we employed a mutant strain of *R. palustris* that constitutively expressed nitrogenase through a manipulation of the NifA protein gene responsible for transcriptional regulation of nitrogenase genes. This modification allowed for extracellular secretion of ammonia and higher resistance to H_2 nitrogenase inhibition. We establish that *S. ovata* and *R. palustris nifA** can be cocultured synergistically to form a robust consortium incubated for longer than 1 mo. The coculture products and dynamics were directed by the substrate gas composition. Furthermore, we employed our model silicon nanowire (SiNW) platform to provide *S. ovata* with reducing equivalents for the reduction of CO_2 to acetate. Subsequent introduction of *R. palustris nifA** to our electrochemical biohybrid system enabled N_2 fixation to ammonia and nitrogenous biomass concurrently. Additionally, *R. palustris nifA** was able to produce PHB from acetate. Finally, our design can be fully sustained with solar energy, establishing a PBS converting H_2O, CO_2, and N_2 renewably in tandem to value-added products.

Results and Discussion

In nature, a symbiosis exists between legume plants and nitrogen-fixing Rhizobia (Fig. 1) (47). Legumes provide an anerobic microenvironment in their root nodules and supply rhizobia with organics, such as malate (48). Rhizobia metabolize the organic substrates and in turn, fix sufficient N_2 for themselves and the host plant. Taking inspiration from nature, we identified the bacterium *R. palustris* that is capable of assimilating acetate to fuel cell functions, including N_2 fixation (49). As demonstrated in *SI Appendix*, Fig. S1, *R. palustris* initiates acetate metabolism by activating acetate to acetyl coenzyme A (acetyl-CoA), which feeds into the tricarboxylic acid (TCA) cycle with a glyoxylate shunt. Acetyl-CoA is combined with oxaloacetate to form citrate. After recombining citrate to isocitrate, it is divided into succinate and glyoxylate. Succinate is oxidized to malate, yielding ubiquinol, while glyoxylate is joined with acetyl-CoA to form malate. Malate is then oxidized to oxaloacetate-generating nicotinamide adenine dinucleotide and ubiquinol. Oxaloacetate is either incorporated back into the TCA cycle or decarboxylated to phosphoenolpyruvate to be used in biosynthesis. In addition to providing ammonia, metabolic N_2 reduction serves as an electron sink allowing for the oxidization of molecular redox shuttles generated through the TCA cycle (50). Therefore, acetate is directly responsible for providing reductive energy to nitrogenase. Concurrently, *R. palustris* could also condense two acetyl-CoA molecules to hydroxybutyryl-CoA, the monomer for PHB.

As a result of the adept acetate metabolism in *R. palustris*, we posit that we could integrate *R. palustris* into our SiNW–*S. ovata* biohybrid system, thus mimicking the plant/bacteria symbiosis fixing both CO_2 and N_2 to value-added products (Fig. 1). Overall, (photo-)electrochemical reducing equivalents power *S. ovata*-mediated CO_2 to acetate conversion; this acetate is then consumed by *R. palustris* to enable N_2 fixation and PHB production.

Characterization of Individual *S. ovata* and *R. palustris nifA Cultures.** Before combining *S. ovata* and *R. palustris*, we characterized each strain's growth and product outputs in separate cultures. We inoculated *S. ovata* in autotrophic medium (pH 6.8,

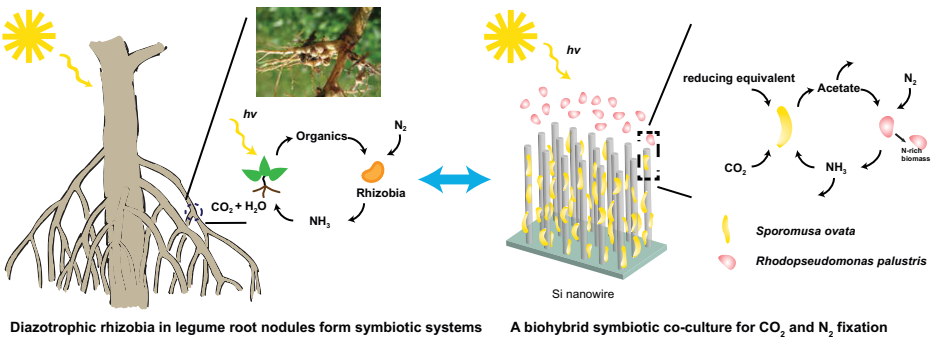

Fig. 1. Bioinspired biohybrid coculture design. Rhizobia inhabit the anoxic root nodules of legumes, where they are provided with organics (e.g., malate) by the legume. The rhizobia in turn fix N_2 to nitrogenous compounds that the legume uses for growth. In our design, an SiNW/*S. ovata* ensemble generates acetate from CO_2, taking the place of the legume. Similar to rhizobia, *R. palustris* uses the acetate as a feedstock to convert N_2 to NH_3. Solar energy powering the biohybrid platform is symbolized by the ray of light where $h\nu$ specifically signifies the light energy. (*Inset*) Image depicts vigna unguiculata root nodules. Image credit: Harry Rose (photographer), licensed under CC BY 2.0.

35 °C) at three sequential starting optical densities (OD): I (starting OD_{545} of 0.15), II (starting OD_{545} of 0.225), and III (starting OD_{545} of 0.6) with an H_2/CO_2 headspace (Fig. 2*A*). Over the first 24 h, III reached an acetate concentration of 34 mM, while I and II reached 25 and 15 mM, respectively (Fig. 2*B*). These results indicated that over the first day, acetate production was proportional to culture density. All cultures achieved a similar acetate concentration on the second day (~52 mM) and a maximum of ~60 mM on the third day, regardless of OD. At this point, the pH of the cultures was 5.2, which is lower than the optimal pH range for *S. ovata* (*SI Appendix*, Fig. S2) (51). The production of acetate presented a self-inhibitive problem; the accumulated acetate became toxic to cells as it acidified the pH of the media to an intolerable level. Each culture set grew by OD_{545} ~ 0.2, and the stationary stage coincided with media acidification, indicating that metabolic activity is paused in a low-pH environment. Therefore, a mechanism for acetate sequestration could maintain a neutral pH and thus, enable sustained growth and metabolic activity of *S. ovata* cultures over a longer period.

Next, we characterized the photoheterotrophic growth of the *R. palustris nifA** mutant under diazotrophic conditions, providing synthetic acetate as a carbon substrate with a pure N_2 headspace. As previously noted, *R. palustris nifA** expresses nitrogenase genes constitutively. This is a result of a mutation in the Q-linker region between the NifA N-terminal GAF and AAA^+ domains (50). The *R. palustris nifA** mutant was first identified by Rey et al. (52) following adaptative evolution to isolate *R. palustris* mutants with enhanced biohydrogen production, as H_2 is produced obligatorily along with NH_3 by nitrogenase. Importantly, the *R. palustris nifA** mutant does not metabolize H_2, which prevents any competition with *S. ovata* for H_2 (53). Secretion of NH_3 into the culture medium by *R. palustris nifA** under N_2-fixing conditions has been previously detected (54). Genetic engineering of the NifA gene has also been undertaken in different N_2-fixing bacteria strains to obtain extracellular NH_3 (55).

We plotted the growth curves of *R. palustris nifA** under diazotrophic conditions provided with increasing acetate concentrations

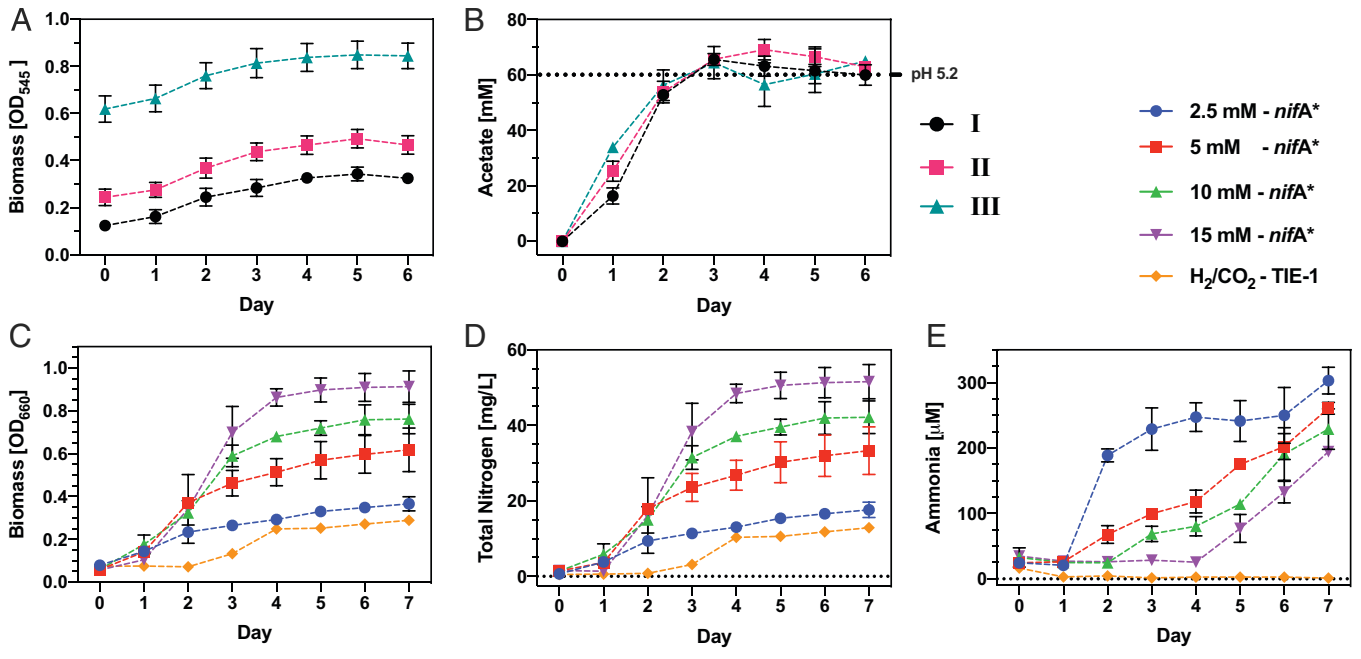

Fig. 2. Monoculture characterization of *S. ovata* and *R. palustris*. (*A*) Biomass and (*B*) acetate tracking of autotrophic *S. ovata* monocultures I, II, and III inoculated at sequentially increasing starting optical densities of OD_{545} = 0.15, OD_{545} = 0.225, and OD_{545} = 0.6, respectively. Diazotrophic, photoheterotrophic *R. palustris nifA** provided with synthetic acetate (2.5 to 15 mM) and photoautotrophic *R.* palustris TIE-1 WT monocultures supplied with an $H_2/CO_2/N_2$ headspace. Daily measurements of (*C*) biomass, (*D*) total nitrogen, and (*E*) ammonia. Error bars represent one SD of three independent measurements.

from 2.5 to 15 mM (Fig. 2*C*). The greatest culture density was achieved in the culture with the highest initial acetate concentration; thus, the biomass production was dictated by acetate. As a comparison, we cultured *R. palustris* TIE-1 wild type (TIE-1 WT) under diazotrophic and autotrophic conditions ($N_2/CO_2/H_2$) (56). *R. palustris* TIE-1 WT failed to reach a comparable density as the photoheterotrophic cultures within the same experimental time frame. Afterward, using a Kjeldahl-type nitrogen digestion assay, we were able to quantify the total fixed nitrogen in each culture set (Fig. 2 *B* and *D*). The amount of fixed nitrogen directly correlated with the density of each culture; thus, the concentration of acetate prescribed the overall quantity of nitrogen that was fixed. We tracked the acetate concentration in an *R. palustris nifA** culture and found that the acetate was categorically consumed by the midexponential phase (*SI Appendix*, Fig. S3). Furthermore, we determined that even if the growth of an *R. palustris nifA** culture plateaus and the initial acetate is completely consumed, we can induce further growth by adding more acetate (*SI Appendix*, Fig. S4). This establishes that *R. palustris nifA** culture activity can be extended by continuous addition of acetate.

Finally, we investigated the ability of *R. palustris nifA** to generate extracellular NH_3. We utilized an established fluorescence-based assay to detect NH_3 coupled with proton nuclear magnetic resonance (^{1}H-NMR) confirmation (57). In order to maximize the amount of NH_3 recovery, we performed a short selection experiment. *R. palustris nifA** was divided into cultures grown photoheterotrophically under diazotrophic conditions, and the culture with the highest concentration of extracellular NH_3 was reinoculated successively over at least five generations (*SI Appendix*, Fig. S5). This boosted the NH_3 recovery by an order of magnitude. We found that the amount of extracellular NH_3 produced by *R. palustris nifA** was inversely proportional to the initially available acetate (i.e., the cultures with 2.5 mM acetate had the highest concentration of extracellular NH_3) (Fig. 2*E*). This observation may be explained by the fact that cultures with higher acetate concentration have access to more carbon for protein biosynthesis through which NH_3 is depleted rapidly. As previously noted, the acetate was fully consumed before the culture reached its maximum OD, pointing to a metabolic stage during which all the acetate has been converted to carbon intermediates. The amount of NH_3 consumed by protein biosynthesis depends on the abundance of carbon intermediates. Therefore, the amount of extracellularly secreted NH_3 decreases with a larger pool of carbon intermediates, which stem from acetate. Nonetheless, more focused study is required to fully elucidate this observation. Favorably, we can conclude that the initial acetate input can be used to direct nitrogen products, either nitrogenous biomass or NH_3. We also conducted an experiment consisting of growing *R. palustris nifA** under varying N_2 headspace pressures (*SI Appendix*, Fig. S6). We confirmed that N_2 pressurization did not have an outsize effect on cell concentration below 175 kPa. The cell concentration at 200 kPa was slightly increased, although experiments at higher pressures could not be safely conducted. The concentration of extracellular NH_3 demonstrated an increasing trend up to 175 kPa. Moreover, we noted H_2 coproduction (247 ± 26 ppm) in N_2-fixing cultures of *R. palustris nifA** as H_2 is an obligatory by-product of nitrogenase-mediated N_2 hydrogenation. We investigated monocultures of *S. ovata* and *R. palustris nifA** to characterize the behavior of each strain under different culturing conditions and to understand how to set up a symbiotic coculture. *R. palustris nifA** could consume acetate generated from CO_2 and H_2 by *S. ovata* and thus, prevent culture acidification, whereas *S. ovata* could benefit by obtaining free NH_3 and H_2 from *R. palustris nifA**-mediated N_2 fixation.

Characterization and Manipulation of *S. ovata* and *R. palustris nifA Cocultures.** Cocultures involving at least one N_2-fixing bacterium have been demonstrated. These consortia have shown the ability of the N_2-fixing strain to provide its partner strain with necessary ammonia. LaSarre et al. (54) established a cross-feeding mutualism, wherein *R. palustris* consumed fermentative products from *E. coli* and subsequently released ammonia promptly taken up by the *E. coli*. Smith and Francis (58) conceived of a coculture in which a genetically engineered photosynthetic cyanobacterium fixed CO_2 and provided an N_2-fixing organism with fixed carbon products. Here, we construct a coculture between *S. ovata* and *R. palustris nifA**. The advantages of our design are the inclusion of *S. ovata*, capable of fixing CO_2 to acetate innately with reducing equivalents sourced from H_2 or from a (photo-)electrochemical process. This lends the ability to direct the coculture products by managing the available substrate gases and the magnitude and duration of the photoelectrochemical process.

We formulated a fixed carbon and nitrogen free minimal medium amenable for both *S. ovata* and *R. palustris nifA** (*SI Appendix*, Fig. S7). Our first approach involved inoculating *S. ovata* and *R. palustris nifA** concurrently in four sets of culture tubes (at OD_{600} of ∼0.4) (Fig. 3 *A* and *C*). The initial cell ratio of *S. ovata* to *R. palustris nifA** was ∼6:1 (determined by correlating OD to cell counts), and the headspace was pressurized to 175 kPa with an $H_2/CO_2/N_2$ (40:20:40%) gas mixture. We tracked OD, acetate, total fixed nitrogen, and ammonia concentrations during the experimental period. Over the course of the experiment, the original headspace gas mixture was exchanged to pure N_2 at different time points in each of the four coculture sets to observe coculture growth dynamics under different headspace conditions. The four coculture sets exhibited similar OD growth over the first 3 d. At this time point, less than 1.25 mM acetate was measured in all respective cocultures, and no ammonia was detected, which pointed to successful cross-feeding. The headspace gas mixture was exchanged to pure N_2 in the first coculture set after 3 d (Fig. 3 *A*, blue curves and *C*, blue bar). By day 10, the remaining three cocultures with $H_2/CO_2/N_2$ headspace continued to exhibit growth more than doubling the initial OD, while the coculture with a pure N_2 headspace showed markedly lower growth rate. Only trace concentrations of acetate and ammonia were detected in all the cocultures. On day 10, the headspace gas mixture in a second coculture was exchanged to pure N_2 (Fig. 3 *A*, red curves and *C*, red bar). By day 19, the two remaining cocultures with $H_2/CO_2/N_2$ headspace had continued their linear growth trend, while the two coculture sets with N_2 headspaces had nearly plateaued. Following this observation, circa 0.5 mM acetate was measured in the cocultures with $H_2/CO_2/N_2$ headspaces, while no acetate could be detected in the cocultures with pure N_2 headspaces, pointing to *S. ovata* inactivity due to the lack of H_2. On day 19, considerable amounts of NH_3 were detected in both cocultures with pure N_2 headspaces, illustrating that NH_3 cross-feeding ceased as *S. ovata* became inactive. The headspace of one of the two remaining cocultures with $H_2/CO_2/N_2$ headspaces was exchanged to pure N_2 on day 19 (Fig. 3 *A*, green curves and *C*, green bar). Final sampling was conducted on day 33 and demonstrated that the coculture with $H_2/CO_2/N_2$ headspace grew to surpass OD_{600} 2.0, while cell densities in the cultures with pure N_2 headspaces plateaued (Fig. 3 *A*, purple curves and *C*, purple bar). The coculture with the $H_2/CO_2/N_2$ headspace proliferated past the densities achieved by either strain in a monoculture. The media did not become acidic as acetate was not allowed to accumulate, which sustained growth of the coculture. Critically, the *S. ovata* in the coculture remained active

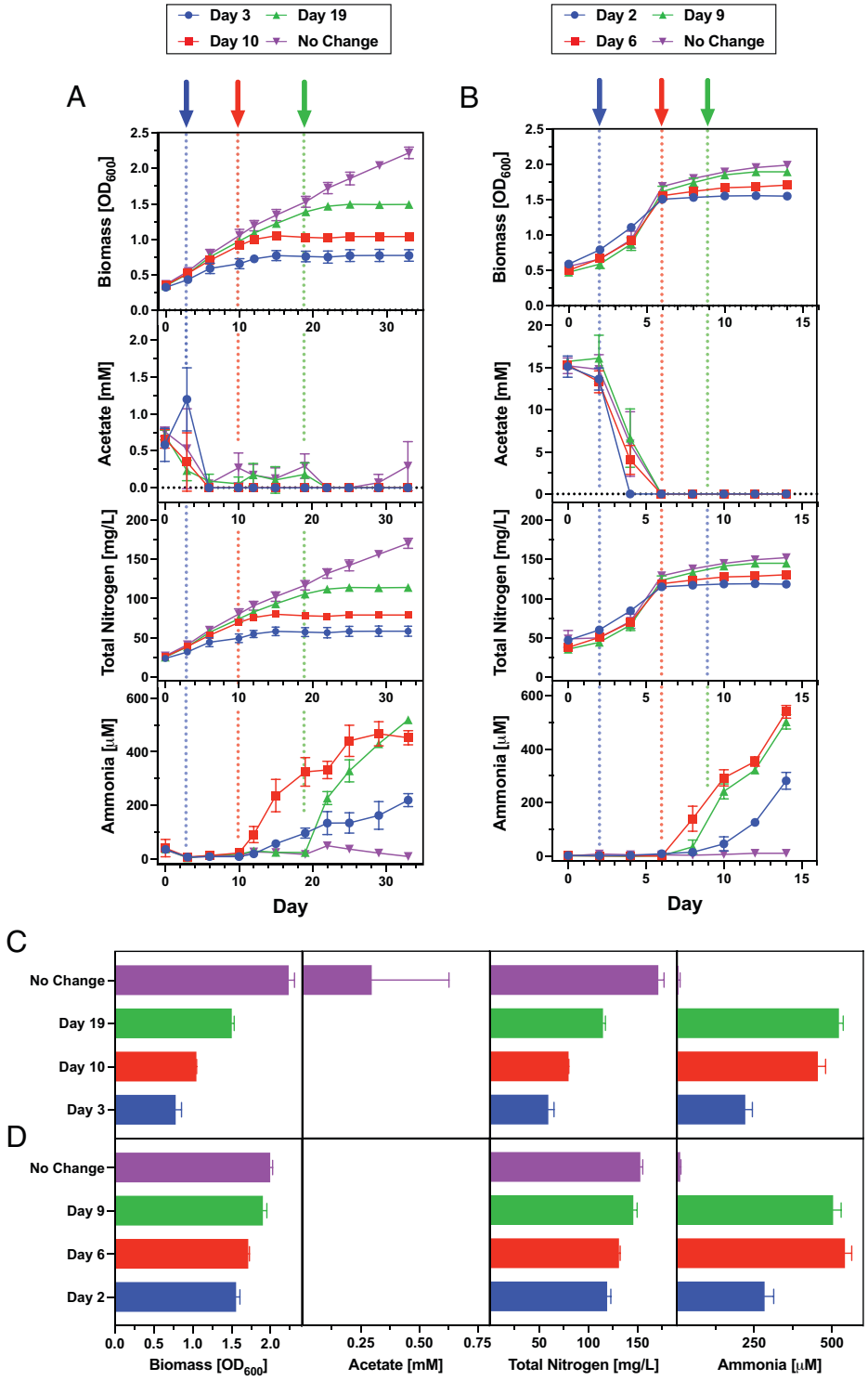

Fig. 3. *S. ovata* and *R. palustris nifA** coculture characterization. (*A*) *S. ovata* and *R. palustris nifA** inoculated concurrently. (*B*) *S. ovata* inoculated 24 h before *R. palustris nifA** is introduced into the culture. The legend signifies the day on which the headspace was exchanged from $H_2/CO_2/N_2$ to pure N_2 for each condition. Color-matching dotted lines and arrows illustrate the day of headspace exchange on each individual plot. *C* and *D* depict the summary of the results on the last sampling day for (*C*) concurrent *S. ovata* and *R. palustris nifA** inoculation and for (*D*) 24-h *S. ovata* incubation prior to *R. palustris nifA** introduction. Error bars represent one SD of three independent measurements.

over the entire 33-d-long experiment if H_2 was available, exhibited by a detectable amount of acetate on the final sampling day and an increase in total fixed nitrogen in the coculture, which was fueled by acetate. Continued coculture growth over >1 mo can be taken as proof of cross-feeding between each species, with *R. palustris nifA** taking up acetate and *S. ovata* consuming ammonia. No significant amount of ammonia could be measured in the coculture with $H_2/CO_2/N_2$ headspace, whereas concentrations in the hundreds of micromolar were measured in the cocultures after they were switched to N_2 headspaces.

While a successful *S. ovata* and *R. palustris nifA** coculture was realized, we sought to accelerate the culturing time with a modified approach. As evidenced by the lack of a typical exponential growth phase in the first cocultures, acetate could be a

limiting factor. Therefore, we inoculated *S. ovata* first with an H_2/CO_2 (80:20%) headspace for 24 h to produce an initial acetate reservoir. Since acetate production for *S. ovata* is a growth-linked process, the pure *S. ovata* cultures were initially provided with 100 μM NH_3 to ensure high acetate production. This supplement was completely consumed within the first 24 h. *R. palustris nifA** is responsible for most of the coculture growth as it grows photoheterotrophically on acetate and *S. ovata* grows autotrophically with limited ammonia. We determined that *S. ovata* has very meager growth when only supplemented with limited NH_3 (*SI Appendix*, Fig. S7*B*). Corroborating this point, LaSarre et al. (54) found that the N_2-fixing organism dominates in an NH_3-deficient coculture, which in their study, was demonstrated as *R. palustris* dominated growth when cocultured with *E. coli*. Therefore, our 24-h preinoculation of *S. ovata* ensured a high acetate concentration (~15 mM) and no extra ammonia upon the introduction of *R. palustris nifA** to accelerate coculture growth (Fig. 3 *B* and *D*). The growth in these cocultures over the first 6 d was exponential in contrast to the first cocultures. Similar to the first coculture experiments, the headspace was exchanged in one coculture on day 2 (Fig. 3 *B*, blue curves, and *D*, blue bar), but the growth continued a similar trajectory as in the others. By day 6, the acetate reservoir had been depleted, and the coculture growth rates slowed down significantly. On days 6 and 9, the second (Fig. 3 *B*, red curves, and *D*, red bar) and third (Fig. 3 *B*, green curves, and *D*, green bar) cocultures had their headspaces exchanged for N_2, respectively. By the final sampling on day 14, the cocultures with an N_2 headspace had plateaued, while the remaining coculture with $H_2/CO_2/N_2$ headspace maintained steady growth, albeit slowed from its initial phase (Fig. 3 *B*, purple curves, and *D*, purple bar). Extracellular ammonia was present in all the cocultures with an N_2 headspace. The 24-h *S. ovata* incubation strategy allowed the coculture to reach an OD_{600} of 2.0 in half the time (14 vs. 28 d). We plotted the densities when the headspaces were exchanged to pure N_2 and performed a regression analysis (*SI Appendix*, Fig. S9). Notably, the slopes of both curves are similar, although the *y* intercept is greater for the curve belonging to the 24-h *S. ovata* preincubation cocultures. This points to comparable steady-state growth dynamics, although prior incubation of *S. ovata* for 24 h grants the coculture much faster initial growth (two times faster biomass accumulation).

Altogether these results indicate that *S. ovata* and *R. palustris nifA** developed a robust consortium with cross-fed acetate and ammonia. Second, coculture dynamics can be directed as evidenced by the changes that occurred after headspace exchange. When reducing equivalents, such as H_2, exist, *S. ovata* supported *R. palustris nifA** with sufficient acetate, resulting in quick consumption of acetate, biomass accumulation, and no free ammonia in the culture. After losing access to H_2, *S. ovata* activity became minimal, and free ammonia by *R. palustris nifA** accumulated due to limited carbon sources.

Electrochemically and Solar-Powered *S. ovata* and *R. palustris nifA-Based CO_2 and N_2 Fixation.** We employed a custom-made H cell–type electrochemical reactor, which we reconditioned with metal clamps and supporting silicone o rings to withstand pressurization. The total volume was 160 mL. A TiO_2- and Ni-coated degenerate SiNW 2.25-cm^2 cathode was fabricated as previously described (17). Pt wire and Ag/AgCl were used as counter and reference electrodes, respectively. The electrolyte was composed as previously noted with some modifications (*SI Appendix*). *S. ovata* was cultured as previously reported, except that the cells were washed three times anaerobically in fresh electrolyte after culturing autotrophically in minimal medium and thereafter, introduced into the cathodic chamber of the electrochemical cell with 100 μM NH_3 mimicking the previous coculture experiment.

We undertook the bioelectrochemical experiments in two stages. First, we generated reducing equivalents on the cathode to power *S. ovata* acetogenesis and produce acetate. Thereafter, we ceased electrochemical inputs and introduced *R. palustris nifA**, which consumed acetate for energy to fix N_2 and produce PHB. We undertook this staged approach to determine productivity and efficiency metrics for each coculture product. For example, if we had inoculated *S. ovata* and *R. palustris nifA** at the same time, we would not have been able to detect acetate, as it would have been instantly consumed by *R. palustris nifA**. Accurately determining the concentration of acetate is paramount in this initial demonstration, as the coculture behaves according to its culturing conditions with acetate concentration directing the makeup of N_2 products, namely NH_3 or nitrogenous biomass.

We allowed for three increasing amounts of charge to pass through the electrodes, as these would translate to increasing acetate outputs (Fig. 4 *A* and *B*). For acetate, the lowest charge (99 ± 12 coulombs) resulted in an FE of 103% with a current density of 0.29 mA/cm^2. Similarly, a charge of 166 ± 20 coulombs translated to an FE of 93% and a current density of 0.35 mA/cm^2, while the experiment with the highest charge of 235 ± 15 coulombs rendered an FE and current density of 91% and 0.35 mA/cm^2, respectively. After *R. palustris nifA** was introduced, the FEs for nitrogen in biomass increased proportionally with charge from 13.7 to 17.4% and to 19.1%. The corresponding current densities demonstrate a similar trend, increasing from 0.049 to 0.058 mA/cm^2 and to 0.067 mA/cm^2. Whereas nitrogenous biomass scaled with charge, NH_3 production revealed a dissimilar trend with the highest FE and current density peaking at 6.3% and 0.023 mA/cm^2, respectively, for 166 ± 20 coulombs. The efficiency of ammonia production fell off with increasing charge. This trend mirrored that of the *R. palustris nifA** monoculture experiment, which exhibited an inverse proportionality between the starting amount of acetate and the concentration of extracellular NH_3 (Fig. 2*E*). Therefore, the nitrogen products can be regarded as tunable because the amount of electrochemical charge passed to the culture dictated their composition. McKinlay and Harwood (59) determined an optimum production yield of 21 ± 3 mol H_2 per 100 mol of acetate fed to *R. palustris nifA**. As H_2 is obligately generated alongside N_2 reduction by nitrogenase, we can stoichiometrically deduce that their nitrogen fixation yield was 42 mol fixed nitrogen per 100 mol acetate. Our *R. palustris nifA** monoculture yielded 31.4 ± 10.5 mol fixed nitrogen per 100 mol acetate, while electrochemical induction results in 28.6 ± 6.8 mol fixed nitrogen per 100 mol acetate. When benchmarking our production metrics with those obtained by McKinlay and Harwood (59), it is apparent that there is an opportunity for improvement, which could increase the average electricity to fixed nitrogen efficiency 1.5-fold.

Importantly, *R. palustris* also synthesized PHB as a form of carbon and energy storage. We measured 1.04 ± 0.04 mg/L PHB (0.8% carbon yield), which was commensurate with previous accounts (60). PHB production could be maximized to up to 30% of the dry cell weight by limiting access to N_2 (49). Therefore, switching to a pure CO_2 headspace (instead of N_2) during coculturing could direct PHB synthesis from acetate, offering more tunable products for this coculture platform. Although not verified in this study, *R. palustris* has been reported to produce

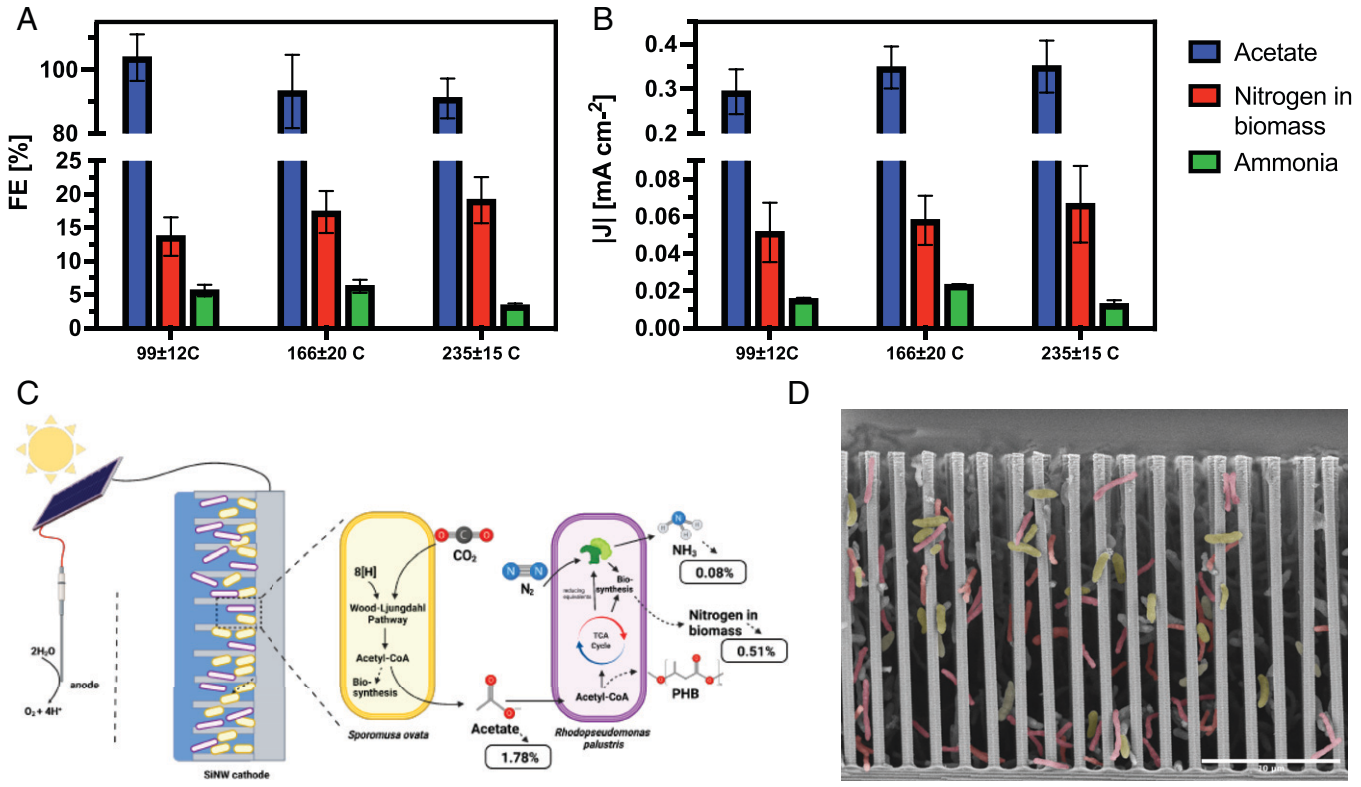

Fig. 4. Electrochemically supported *S. ovata* and *R. palustris nifA**. (*A* and *B*) FEs and current densities for coculture products acetate, nitrogenous biomass, and ammonia. (*C*) Fully solar-powered coculture via an external photovoltaic device with solar to chemical efficiencies. (*D*) Scanning electron microscopy micrograph of the SiNW array with *S. ovata* and *R. palustris nifA**. Individual bacteria on the front-most plane are identified and color-highlighted based on morphology (*S. ovata* is yellow, and *R. palustris* is pink). Error bars represent one SD of three independent measurements.

CH_4 simultaneously with NH_3, thus possibly positioning the coculture platform to offer another carbon product (61). Additionally, other forms of exploitable carbon storage products have also been observed for *R. palustris*, including glycogen and trehalose (49). Moreover, isotope-labeled ^{13}C control experiments were employed (*SI Appendix*, Fig. S10). To further confirm N_2 fixation, we inoculated *R. palustris nifA** into liquid cultures with argon (Ar) degassed medium. We then filled the headspaces with $^{15}N_2$ and Ar and provided acetate to each. Notably, the culture with Ar exhibited negligible growth, and the culture with $^{15}N_2$ accumulated biomass through $^{15}N_2$ fixation (*SI Appendix*, Fig. S11*A*). ^{1}H-NMR results confirm no $^{14}NH_3$ in the Ar culture and $^{15}NH_3$ in the $^{15}N_2$ culture (*SI Appendix*, Fig. S11*B*). The absence of $^{14}NH_3$ in cultures with Ar and $^{15}N_2$ headspaces and the lack of growth in the Ar culture point to curtailed external contaminations.

Following the confirmation of an electrochemically supported platform, we investigated whether our system would allow for solar-driven CO_2 and N_2 fixation. We connected our electrochemical cell housing the bacterial coculture to a photovoltaic device, as shown in diagram in Fig. 4*C*, and followed a process analogous to the electrochemical experiments. Similarly to our previous report, we used a commercially available multijunction Si solar cell (V_{oc} = 4.7 V, I_{sc} = 4.4 mA under one sun illumination) to drive the reaction (17). The light intensity was set at 25 mWcm^{-2} using an National Renewable Energy Laboratory (NREL)-calibrated Si photodiode. The system produced acetate with a solar to chemical efficiency of 1.78 ± 0.13% over 2 d, and upon introduction of *R. palustris nifA**, it was able to fix N_2 into nitrogenous biomass and ammonia with efficiencies of 0.51 ± 0.05% and 0.08 ± 0.007%, correspondingly. To the best of our knowledge, no other platform has been reported for full solar-driven CO_2 and N_2 fixation.

Finally, we assessed the SiNW array used to support the bacterial culture by scanning electron microscopy. We noticed the presence of two distinct bacterial morphologies. One was bulbous, and the other was more tubular in appearance. We proceeded to culture *R. palustris nifA** and *S. ovata* individually on SiNWs and examined them by scanning electron microscopy (*SI Appendix*, Fig. S12 *A* and *B*). We observed that the bulbous morphology can be attributed to *S. ovata*, while *R. palustris nifA** presents as longer and thinner. These observations of the individual strain morphologies agree with the literature (51, 52). Next, we centrifuged down a mature coculture at 12,000 rpm and found layering, with the longer, heavier, and pink *R. palustris nifA** underneath the shorter, lighter, and beige *S. ovata* as evident by the distinct colors of each strain (*SI Appendix*, Fig. S12*C*). A qualitative approximation of the final cell ratio is 2:3 *S. ovata* to *R. palustris nifA**, having been seeded at an initial 6:1 *S. ovata* to *R. palustris nifA** cell ratio. This result corroborates that most of the coculture growth stems from the N_2-fixing heterotrophic *R. palustris*, as has previously been claimed (54). Finally, we were able to qualitatively identify each bacterial strain on the front-most plane of a scanning electron microscopy micrograph as highlighted by false coloring in Fig. 4*D* (*SI Appendix*, Fig. S12*D*). Fluorescence-activated cell sorting or a fluorescence in situ hybridization assay needs to be performed to quantitatively report individual bacterial populations in future work.

Overall, we demonstrate a biohybrid coculture capable of fixing CO_2 and N_2 to value-added products. We namely show that bio-produced acetate from CO_2 could be used to power N_2 fixation in a separate whole-cell catalyst. By assigning CO_2 and N_2 fixation to two separate biocatalysts, we are able to maximize efficiency and rate. However, not only is acetate a

fuel for N_2 fixation, but it also provides a substrate for bioplastic synthesis and potentially manifold other carbon products owing to the metabolic versatility of *R. palustris*. Moreover, employing two separate biocatalysts in synergy allowed us to direct product outputs through electrochemistry and headspace inputs. We strongly believe that advances in bioelectrochemistry will arise from studying and engaging bacterial communities. Organisms in nature cooperate to thrive, and we must emulate these associations in biohybrid systems to tackle environmental challenges.

Materials and Methods

Cell Culture. Balch-type anaerobic culture tubes with butyl stoppers were employed to separate the culture from the environment and maintain desired headspace pressure. A COY vinyl anaerobic chamber was used to conduct experiments anaerobically. *S. ovata* was purchased from the American Type Culture Collection (35899) and rehydrated as indicated. It was then grown in betaine medium and aliquoted with dimethyl sulfoxide as a cryoprotectant to be stored at −80 °C. Frozen cells were revived in betaine medium and cultured for two cycles before inoculating in yeast medium. *S. ovata* from yeast medium was inoculated at 5% (vol/vol) in autotrophic medium with H_2/CO_2 80:20% headspace at 175 kPA. *S. ovata* was incubated at 35 °C in starting pH 7.2. Frozen stocks of *R. palustris* strains TIE-1 (56) and *nifA** as prepared in McKinlay and Harwood (50) provided by the Harwood group (Caroline Harwood, University of Washington, Seattle, WA) were inoculated in photoheterotrophic medium supplemented with 20 mM acetate for two cycles. The cells were washed three times anaerobically before inoculating in diazotrophic photoheterotrophic medium (N_2 100% headspace) or diazotrophic autotrophic medium ($H_2/CO_2/N_2$ 40:20:40% headspace). *R. palustris* was incubated at 30 °C in starting pH 6.8 with a 20-W compact flourescent light bulb. *S. ovata/R. palustris* cocultures were cultivated in coculture medium. *S. ovata* was typically inoculated first from an autotrophic culture after three anaerobic washes to remove nitrogen. *R. palustris* was added thereafter also after three anaerobic washes. The coculture was maintained at 30 °C with a 20-W compact fluorescent light bulb with headspace as indicated in the experiment.

Analysis of Acetate, Ammonia, Total Nitrogen, and Hydrogen. Acetate concentration was assessed by proton quantitative nuclear magnetic resonance (^{1}H-qNMR) spectroscopy (Bruker 400 MHz) with sodium 3-(trimethylsilyl)-2,2′,3,3′-tetradeuteropropionate as the internal standard. The ^{13}C-labeled experiment was conducted as previously reported (18). Ammonia was determined by the *o*-phthalaldehyde (OPA) method as previously reported with slight modifications (57); 100 mg OPA was dissolved in 3.125 mL pure ethanol, and 50 mL 0.2 M sodium tetraborate buffer was prepared with 1.3 mM sodium sulfite. The two solutions were mixed quickly avoiding light exposure. These reagents were prepared fresh before experiments. Cell culture samples were ultracentrifuged and filtered to separate the cell material from the supernatant. The supernatant and reagent solution were combined in a 1:10 ratio and assayed with a fluorescence-equipped plate reader (SpectraMax i3x; $\lambda_{ex} = 410$ nm, $\lambda_{em} = 470$ nm). Ammonia was also routinely verified with a commercial testing kit (HACH TNT830) as per the manufacturer's instruction. Ammonia and ^{15}N-labeled experiments were assayed by ^{1}H-qNMR spectroscopy (Bruker 500 MHz) with water suppression. Cell culture media were degassed with Ar, and the cell culture vessel headspace was evacuated after sealing under Ar atmosphere. Total fixed nitrogen was determined as per a previous report (38) using a commercial persulfate nitrogen digestion kit (Hach Company 2672245). The samples were ultracentrifuged to separate the supernatant from the cell material. The cell material was washed before using the nitrogen digestion kit. Total nitrogen as a function of cell counts and OD calibration curves were established spectrophotometrically for experimental sets as needed. Hydrogen production in diazotrophic cultures was quantified by gas chromatography after 24 h (Agilent 7890B GC system). PHB content was quantified as per Wang et al. (62). First-cell PHB content was hydrolyzed with NaOH under heating, and then, a β-Hydroxybutyrate Assay Kit (Sigma Aldrich MAK041) was used for spectrophotometric quantification.

Electrochemical- and Solar-Driven Experiments. p^+ Si nanowire array electrodes were prepared as previously described (17). Briefly, the Si nanowire arrays were etched from 6-inch p^+-Si (boron) wafers ($\rho \sim 0.001$ to 0.005 Ω·cm) after patterning with a photoresist dot array using a standard photolithography stepper. They were then coated with 5 nm of TiO_2 as a protective layer by atomic layer deposition (Picosun ALD). Finally, they were sputtered with ∼10 nm nickel (Edwards Inc.). The Si nanowire wafer was cut to 2.25-cm^2 pieces and placed on a Ti foil with Ga-In eutectic, silver glue, and carbon tape to maintain electrical contact. A water-resistant rubber resin (Gardner Bender) was used to seal the backside and sides of the Si electrode. A homemade closed chamber H cell–type electrochemical cell equipped with mechanical clamps to maintain pressure was filled with 160 mL of coculture electrolyte (80 mL in each of the cathodic and anodic chambers) and a 175-kPa CO_2/N_2 headspace. Fresh Nafion 117 membranes were pretreated with 5% H_2O_2 and rinsed with ultrapure water directly before each experiment. The H cell was sonicated in dilute HCl to sterilize. *S. ovata* was cultured in autotrophic medium with an H_2/CO_2 headspace, and 36 h prior to the electrochemical experiment, the headspace was exchanged to CO_2/N_2. Typically, electrochemical bias was started 24 h before introducing *S. ovata* to the H cell with an Ag/AgCl (1 M KCl) reference and Pt wire as a counter and conducted with Gamry Interface 1,000 potentiostats. The *S. ovata* in autotrophic medium was washed three times and introduced into the cathodic chamber. The electrochemical bias (∼−0.3 V vs. reversible hydrogen electrode, medium pH 6.8) was maintained until a specified amount of charge was passed. Afterward, three time–washed *R. palustris nif*A* was inoculated into the cathodic chamber. For the solar-driven experiments, a two-electrode configuration was used as per previous experiments, where the SiNW electrode served as the cathode and the Pt wire served as the anode (17). A commercial single-crystalline 0.96-cm^2 Si solar cell (KXOB22-01x8F) was purchased from Digi-key Corporation, and a 300-W xenon arc lamp (Newport Corporation) with an AM1.5G filter was used for illumination. An Si photodiode referenced to an NREL-calibrated photodiode was employed to calibrate the light intensity to 25 mW/cm^2. Samples were evaluated for acetate, ammonia, total nitrogen in biomass, and PHB as described.

$FE_{acetate}$ was calculated based on the following equation:

$$FE_{acetate} = \frac{96,485\ \frac{C}{\text{mol}} \times 8\ (e^-) \times \text{moles}}{\text{charge passed (C)}} \times 100\%.$$

The specific CO_2-reducing current density (per electrode area) $J_{acetate}$ is defined as

$$J_{acetate} = FE_{acetate} \times J_{total},$$

where J_{total} is the average stabilized current during chronoamperometry.

$FE_{nitrogen\ in\ biomass}$ and $FE_{nitrogen\ in\ biomass}$ were calculated based on the following equations (assuming no H_2 recycling as *R. palustris nif*A* is incapable of metabolizing H_2):

$$FE_{nitrogen\ in\ biomass} = \frac{96,485\ \frac{C}{\text{mol}} \times 4\ (e^-) \times [N_{final}\frac{g}{L} - N_{initial}\frac{g}{L}] \times \text{V(L)}}{14\frac{g}{\text{mol}} \times \text{charge passed (C)}} \times 100\%.$$

The specific N_2-reducing current density (per electrode area) $J_{nitrogen\ in\ biomass}$ is defined as

$$J_{nitrogen\ in\ biomass} = FE_{nitrogen\ in\ biomass} \times J_{total}.$$

$$FE_{ammonia} = \frac{96.485\ \frac{C}{\text{mol}} \times 4\ (e^-) \times \text{moles}}{\text{charge passed (C)}} \times 100\%.$$

The specific N_2-reducing current density (per electrode area) $J_{ammonia}$ is defined as

$$J_{ammonia} = FE_{ammonia} \times J_{total}.$$

Total solar to chemical efficiencies were calculated as follows for C and N products, where 1.09 and 1.14 V are the respective thermodynamic potentials needed to microbially reduce CO_2 and N_2 to acetate and ammonia (18, 38, 63):

$$\eta_{acetate} = \frac{1.09\text{V} \times J_{acetate}\ \frac{\text{mA}}{\text{cm}^2} \times A_{electrode}\ \text{cm}^2}{\text{I}\ \frac{\text{mW}}{\text{cm}^2} \times A_{solar\ cell}\ \text{cm}^2} \times 100\%$$

$$\eta_N = \frac{1.14\text{V} \times J_N\ \frac{\text{mA}}{\text{cm}^2} \times A_{electrode}\ \text{cm}^2}{\text{I}\ \frac{\text{mW}}{\text{cm}^2} \times A_{solar\ cell}\ \text{cm}^2} \times 100\%.$$

Scanning Electron Microscopy Characterization. Bacterial cultures were supplemented with glutaraldehyde at 2.5% (vol/vol) and kept at room temperature

overnight. The cells embedded in the SiNW substrates were washed and consecutively dehydrated with 10, 25, 50, 75, 90, and 100% ethanol each for 10 min. The ensembles were immersed in hexamethyldisilazide for 2 h and thereafter, allowed to dry overnight. The ensembles were cut in half, sputtered with gold (Denton Vacuum, LLC), and finally, imaged at 5 keV/12 μA by field emission scanning electron microscopy (JEOL FSM6430).

Data Availability. All study data are included in the article and/or *SI Appendix*.

ACKNOWLEDGMENTS. This work was supported by NASA Grant NNX17AJ31G. We thank Dr. Michael Ross, Dr. Yifan Li, Inwhan Roh, Kyle Valgardson, and Mathangi Soundararajan for helpful discussions and Dr. Jessica Spradlin for assistance with plate fluorescence measurements. We recognize Professor Caroline Harwood's group at the University of Washington for providing the *R. palustris* strains used in this work and the Marvell Nanofabrication Laboratory for use of their facilities. We also thank the staff at the University of California, Berkeley's NMR facility in the College of Chemistry (CoC) for spectroscopic assistance. Instruments in the CoC-NMR are supported in part by NIH Grant S10OD024998. We also recognize the glassblowing shop at the CoC for assistance with fabricating the H cell. S.C.-B. thanks the Philomathia Foundation for a personal fellowship. R.R.C. thanks the University of California, Berkeley Amgen Scholar Program for support. S.Y. acknowledges support from the Samsung Graduate Fellowship.

Author affiliations: [a]Department of Materials Science and Engineering, University of California, Berkeley, CA 94720; [b]Center for the Utilization of Biological Engineering in Space, University of California, Berkeley, CA 94720; [c]Department of Chemistry, University of California, Berkeley, CA 94720; [d]Department of Applied Physics, Eindhoven University of Technology, Eindhoven, 5600 MB, The Netherlands; [e]Department of Chemistry and Biochemistry, Utah State University, Logan, UT 84322; [f]Chemical Sciences Division, Lawrence Berkeley National Laboratory, Berkeley, CA 94720; and [g]Kavli Energy Nanosciences Institute, Berkeley, CA 94720

1. J. W. Erisman, M. A. Sutton, J. Galloway, Z. Klimont, W. Winiwarter, How a century of ammonia synthesis changed the world. *Nat. Geosci.* **1**, 636–639 (2008).
2. D. Kim, K. K. Sakimoto, D. Hong, P. Yang, Artificial photosynthesis for sustainable fuel and chemical production. *Angew. Chem. Int. Ed. Engl.* **54**, 3259–3266 (2015).
3. M. B. Ross *et al.*, Designing materials for electrochemical carbon dioxide recycling. *Nat. Catal.* **2**, 648–658 (2019).
4. H. Chen, F. Dong, S. D. Minteer, The progress and outlook of bioelectrocatalysis for the production of chemicals, fuels and materials. *Nat. Catal.* **3**, 225–244 (2020).
5. T. Haas, R. Krause, R. Weber, M. Demler, G. Schmid, Technical photosynthesis involving CO_2 electrolysis and fermentation. *Nat. Catal.* **1**, 32–39 (2018).
6. K. Rabaey, R. A. Rozendal, Microbial electrosynthesis–revisiting the electrical route for microbial production. *Nat. Rev. Microbiol.* **8**, 706–716 (2010).
7. N. Kornienko, J. Z. Zhang, K. K. Sakimoto, P. Yang, E. Reisner, Interfacing nature's catalytic machinery with synthetic materials for semi-artificial photosynthesis. *Nat. Nanotechnol.* **13**, 890–899 (2018).
8. N. J. Claassens, D. Z. Sousa, V. A. P. M. Dos Santos, W. M. de Vos, J. van der Oost, Harnessing the power of microbial autotrophy. *Nat. Rev. Microbiol.* **14**, 692–706 (2016).
9. J. Luo *et al.*, Water photolysis at 12.3% efficiency via perovskite photovoltaics and Earth-abundant catalysts. *Science* **345**, 1593–1596 (2014).
10. J. He, C. Janáky, Recent advances in solar-driven carbon dioxide conversion: Expectations versus reality. *ACS Energy Lett.* **5**, 1996–2014 (2020).
11. S. Cestellos-Blanco, H. Zhang, J. M. Kim, Y. Shen, P. Yang, Photosynthetic semiconductor biohybrids for solar-driven biocatalysis. *Nat. Catal.* **3**, 245–255 (2020).
12. K. P. Nevin *et al.*, Electrosynthesis of organic compounds from carbon dioxide is catalyzed by a diversity of acetogenic microorganisms. *Appl. Environ. Microbiol.* **77**, 2882–2886 (2011).
13. K. P. Nevin, T. L. Woodard, A. E. Franks, Z. M. Summers, D. R. Lovley, Microbial electrosynthesis: Feeding microbes electricity to convert carbon dioxide and water to multicarbon extracellular organic compounds. *MBio* **1**, e00103-10 (2010).
14. C. Liu, B. C. Colón, M. Ziesack, P. A. Silver, D. G. Nocera, Water splitting-biosynthetic system with CO_2 reduction efficiencies exceeding photosynthesis. *Science* **352**, 1210–1213 (2016).
15. H. Huang *et al.*, CRISPR/Cas9-based efficient genome editing in *Clostridium ljungdahlii*, an autotrophic gas-fermenting bacterium. *ACS Synth. Biol.* **5**, 1355–1361 (2016).
16. P. L. Tremblay, D. Höglund, A. Koza, I. Bonde, T. Zhang, Adaptation of the autotrophic acetogen *Sporomusa ovata* to methanol accelerates the conversion of CO_2 to organic products. *Sci. Rep.* **5**, 16168 (2015).
17. Y. Su *et al.*, Close-packed nanowire-bacteria hybrids for efficient solar-driven CO_2 Fixation. *Joule* **4**, 800–811 (2020).
18. C. Liu *et al.*, Nanowire-bacteria hybrids for unassisted solar carbon dioxide fixation to value-added chemicals. *Nano Lett.* **15**, 3634–3639 (2015).
19. D. S. Ripatti, T. R. Veltman, M. W. Kanan, Carbon monoxide gas diffusion electrolysis that produces concentrated C_2 products with high single-pass conversion. *Joule* **3**, 240–256 (2019).
20. A. Prévoteau, J. M. Carvajal-Arroyo, R. Ganigué, K. Rabaey, Microbial electrosynthesis from CO_2: Forever a promise? *Curr. Opin. Biotechnol.* **62**, 48–57 (2020).
21. B. Molitor, A. Mishra, L. T. Angenent, Power-to-protein: Converting renewable electric power and carbon dioxide into single cell protein with a two-stage bioprocess. *Energy Environ. Sci.* **12**, 3515–3521 (2019).
22. P. Hu *et al.*, Integrated bioprocess for conversion of gaseous substrates to liquids. *Proc. Natl. Acad. Sci. U.S.A.* **113**, 3773–3778 (2016).
23. S. Cestellos-Blanco *et al.*, Production of PHB from CO_2-derived acetate with minimal processing assessed for space biomanufacturing. *Front. Microbiol.* **12**, 700010 (2021).
24. X. Liu *et al.*, Syntrophic interspecies electron transfer drives carbon fixation and growth by *Rhodopseudomonas palustris* under dark, anoxic conditions. *Sci. Adv.* **7**, eabh1852 (2021).
25. E. V. LaBelle, C. W. Marshall, H. D. May, Microbiome for the electrosynthesis of chemicals from carbon dioxide. *Acc. Chem. Res.* **53**, 62–71 (2020).
26. C. W. Marshall, D. E. Ross, E. B. Fichot, R. S. Norman, H. D. May, Long-term operation of microbial electrosynthesis systems improves acetate production by autotrophic microbiomes. *Environ. Sci. Technol.* **47**, 6023–6029 (2013).
27. X. Fang, S. Kalathil, G. Divitini, Q. Wang, E. Reisner, A three-dimensional hybrid electrode with electroactive microbes for efficient electrogenesis and chemical synthesis. *Proc. Natl. Acad. Sci. U.S.A.* **117**, 5074–5080 (2020).
28. D. R. MacFarlane *et al.*, A roadmap to the ammonia economy. *Joule* **4**, 1186–1205 (2020).
29. C. Smith, L. Torrente-Murciano, The potential of green ammonia for agricultural and economic development in Sierra Leone. *One Earth* **4**, 104–113 (2021).
30. G. Soloveichik, Electrochemical synthesis of ammonia as a potential alternative to the Haber–Bosch process. *Nat. Catal.* **2**, 377–380 (2019).
31. Y. C. Hao *et al.*, Promoting nitrogen electroreduction to ammonia with bismuth nanocrystals and potassium cations in water. *Nat. Catal.* **2**, 448–456 (2019).
32. N. Lazouski, M. Chung, K. Williams, M. L. Gala, K. Manthiram, Non-aqueous gas diffusion electrodes for rapid ammonia synthesis from nitrogen and water-splitting-derived hydrogen. *Nat. Catal.* **3**, 463–469 (2020).
33. A. R. Singh *et al.*, Strategies toward selective electrochemical ammonia synthesis. *ACS Catal.* **9**, 8316–8324 (2019).
34. B. H. R. Suryanto *et al.*, Challenges and prospects in the catalysis of electroreduction of nitrogen to ammonia. *Nat. Catal.* **2**, 290–296 (2019).
35. Y. Liu *et al.*, Facile ammonia synthesis from electrocatalytic N_2 reduction under ambient conditions on N-doped porous carbon. *ACS Catal.* **8**, 1186–1191 (2018).
36. K. Zhang, R. Guo, F. Pang, J. He, W. Zhang, Low-coordinated gold atoms boost electrochemical nitrogen reduction reaction under ambient conditions. *ACS Sustain. Chem. Eng.* **7**, 10214–10220 (2019).
37. Z. H. Xue *et al.*, Electrochemical reduction of N_2 into NH_3 by donor-acceptor couples of Ni and Au nanoparticles with a 67.8% Faradaic efficiency. *J. Am. Chem. Soc.* **141**, 14976–14980 (2019).
38. C. Liu, K. K. Sakimoto, B. C. Colón, P. A. Silver, D. G. Nocera, Ambient nitrogen reduction cycle using a hybrid inorganic-biological system. *Proc. Natl. Acad. Sci. U.S.A.* **114**, 6450–6455 (2017).
39. M. Soundararajan *et al.*, Phototrophic N_2 and CO_2 fixation using a *Rhodopseudomonas palustris*-H_2 mediated electrochemical system with infrared photons. *Front. Microbiol.* **10**, 1817 (2019).
40. S. Lu *et al.*, Perfluorocarbon nanoemulsions create a beneficial O_2 microenvironment in N2-fixing biological | inorganic hybrid. *Chem. Catalysis* **1**, 704–720 (2021).
41. S. Lu, X. Guan, C. Liu, Electricity-powered artificial root nodule. *Nat. Commun.* **11**, 1–10 (2020).
42. F. Dong, Y. S. Lee, E. M. Gaffney, W. Liou, S. D. Minteer, Engineering cyanobacterium with transmembrane electron transfer ability for bioelectrochemical nitrogen fixation. *ACS Catal.* **11**, 13169–13179 (2021).
43. M. E. Rasche, D. J. Arp, Hydrogen inhibition of nitrogen reduction by nitrogenase in isolated soybean nodule bacteroids. *Plant Physiol.* **91**, 663–668 (1989).
44. B. K. Burgess, S. Wherland, W. E. Newton, E. I. Stiefel, Nitrogenase reactivity: Insight into the nitrogen-fixing process through hydrogen-inhibition and HD-forming reactions. *Biochemistry* **20**, 5140–5146 (1981).
45. F. W. Larimer *et al.*, Complete genome sequence of the metabolically versatile photosynthetic bacterium *Rhodopseudomonas palustris*. *Nat. Biotechnol.* **22**, 55–61 (2004).
46. M. A. Vigil Fuentes *et al.*, Study on the 3D printability of poly(3-hydroxybutyrate-co-3-hydroxyvalerate)/poly(lactic acid) blends with chain extender using fused filament fabrication. *Sci. Rep.* **10**, 11804 (2020).
47. J. E. Beringer, N. Brewin, A. W. B. Johnston, H. M. Schulman, D. A. Hopwood, The Rhizobium-legume symbiosis. *Proc. R. Soc. Lond. Biol. Sci.* **204**, 219–233 (1979).
48. A. R. Schwember, J. Schulze, A. Del Pozo, R. A. Cabeza, Regulation of symbiotic nitrogen fixation in legume root nodules. *Plants* **8**, 333 (2019).
49. J. B. McKinlay *et al.*, Non-growing *Rhodopseudomonas palustris* increases the hydrogen gas yield from acetate by shifting from the glyoxylate shunt to the tricarboxylic acid cycle. *J. Biol. Chem.* **289**, 1960–1970 (2014).
50. J. B. McKinlay, C. S. Harwood, Carbon dioxide fixation as a central redox cofactor recycling mechanism in bacteria. *Proc. Natl. Acad. Sci. U.S.A.* **107**, 11669–11675 (2010).
51. B. Möller, R. Oßmer, B. H. Howard, G. Gottschalk, H. Hippe, *Sporomusa*, a new genus of gram-negative anaerobic bacteria including *Sporomusa sphaeroides* spec. nov. and *Sporomusa ovata* spec. nov. *Arch. Microbiol.* **139**, 388–396 (1984).
52. F. E. Rey, E. K. Heiniger, C. S. Harwood, Redirection of metabolism for biological hydrogen production. *Appl. Environ. Microbiol.* **73**, 1665–1671 (2007).
53. A. Adessi, J. B. McKinlay, C. S. Harwood, R. De Philippis, A *Rhodopseudomonas palustris* nifA* mutant produces H_2 from NH_4^+-containing vegetable wastes. *Int. J. Hydrogen Energy* **37**, 15893–15900 (2012).
54. B. LaSarre, A. L. McCully, J. T. Lennon, J. B. McKinlay, Microbial mutualism dynamics governed by dose-dependent toxicity of cross-fed nutrients. *ISME J.* **11**, 337–348 (2017).
55. Y. Ding *et al.*, Nanorg microbial factories: Light-driven renewable biochemical synthesis using quantum dot-bacteria nanobiohybrids. *J. Am. Chem. Soc.* **141**, 10272–10282 (2019).
56. Y. Jiao, A. Kappler, L. R. Croal, D. K. Newman, Isolation and characterization of a genetically tractable photoautotrophic Fe(II)-oxidizing bacterium, *Rhodopseudomonas palustris* strain TIE-1. *Appl. Environ. Microbiol.* **71**, 4487–4496 (2005).
57. H. Hu, Y. Liang, S. Li, Q. Guo, C. Wu, A modified *o*-phthalaldehyde fluorometric analytical method for ultratrace ammonium in natural waters using EDTA-NaOH as buffer. *J. Anal. Methods Chem.* **2014**, 728068 (2014).

58. M. J. Smith, M. B. Francis, A designed *A. vinelandii-S. elongatus* coculture for chemical photoproduction from air, water, phosphate, and trace metals. *ACS Synth. Biol.* **5**, 955–961 (2016).
59. J. B. McKinlay, C. S. Harwood, Calvin cycle flux, pathway constraints, and substrate oxidation state together determine the H_2 biofuel yield in photoheterotrophic bacteria. *MBio* **2**, e00323-10 (2011).
60. T. O. Ranaivoarisoa, R. Singh, K. Rengasamy, M. S. Guzman, A. Bose, Towards sustainable bioplastic production using the photoautotrophic bacterium *Rhodopseudomonas palustris* TIE-1. *J. Ind. Microbiol. Biotechnol.* **46**, 1401–1417 (2019).
61. Y. Zheng *et al.*, A pathway for biological methane production using bacterial iron-only nitrogenase. *Nat. Microbiol.* **3**, 281–286 (2018).
62. B. Wang, Z. Jiang, J. C. Yu, J. Wang, P. K. Wong, Enhanced CO_2 reduction and valuable C_{2+} chemical production by a CdS-photosynthetic hybrid system. *Nanoscale* **11**, 9296–9301 (2019).
63. V. P. Gutschick, "Energetics of microbial fixation of dinitrogen" in *Microbes and Engineering Aspects*, A. Fiechter, Ed. (Advances in Biochemical Engineering, Springer, Berlin, Germany, 1982), vol. **21**, pp. 109–167.